On Integrated Access and Backhaul Networks: Current Status and Potentials

CHARITHA MADAPATHA [1], **BEHROOZ MAKKI** [2] (Senior Member, IEEE), **CHAO FANG** [1],
OUMER TEYEB[3] (Member, IEEE), **ERIK DAHLMAN**[3], **MOHAMED-SLIM ALOUINI** [4] (Fellow, IEEE),
AND TOMMY SVENSSON [1] (Senior Member, IEEE)

[1]Department of Electrical Engineering, Chalmers University of Technology, 412 96 Gothenburg, Sweden

[2]Ericsson Research, 417 56 Gothenburg, Sweden

[3]Ericsson Research, 164 40 Kista, Sweden

[4]Computer, Electrical and Mathematical Science and Engineering, King Abdullah University of Science and Technology, Thuwal 23955-6900, Saudi Arabia

CORRESPONDING AUTHOR: B. MAKKI (e-mail: behrooz.makki@ericsson.com)

ABSTRACT In this article, we introduce and study the potentials and challenges of integrated access and backhaul (IAB) as one of the promising techniques for evolving 5G networks. We study IAB networks from different perspectives. We summarize the recent Rel-16 as well as the upcoming Rel-17 3GPP discussions on IAB, and highlight the main IAB-specific agreements on different protocol layers. Also, concentrating on millimeter wave-based communications, we evaluate the performance of IAB networks in both dense and suburban areas. Using a finite stochastic geometry model, with random distributions of IAB nodes as well as user equipments (UEs) in a finite region, we study the service coverage rate defined as the probability of the event that the UEs' minimum rate requirements are satisfied. We present comparisons between IAB and hybrid IAB/fiber-backhauled networks where a part or all of the small base stations are fiber-connected. Finally, we study the robustness of IAB networks to weather and various deployment conditions and verify their effects, such as blockage, tree foliage, rain as well as antenna height/gain on the coverage rate of IAB setups, as the key differences between the fiber-connected and IAB networks. As we show, IAB is an attractive approach to enable the network densification required by 5G and beyond.

INDEX TERMS Integrated access and backhaul, IAB, densification, millimeter wave (mmWave) communications, 3GPP, stochastic geometry, Poisson point process, coverage probability, germ-grain model, ITU-R, FITU-R, wireless backhaul, 5G NR, rain, tree foliage, blockage, relay.

I. INTRODUCTION

DIFFERENT reports, e.g., [1], predict a steep increase of Internet devices connected through wireless access as well as a massive increase in mobile traffic. To cope with such requirements, along with utilizing more spectrum, the fifth generation (5G) wireless networks and beyond propose different ways for spectral efficiency and capacity improvements. Network densification [2], [3] is one of the key enablers among the alternative approaches, e.g., various distributed antenna systems techniques, including cell-free massive multiple-input-multiple-output (MIMO) and can be achieved via the deployment of many access points of different types, so that there are more resource blocks per unit area.

The base stations (BSs) need to be connected to the operators' core network via a transport network. A transport network may consist of wired or wireless connections. Typically, wireless connections are used for backhaul transport in the radio access network (RAN), closer to the BSs, while wired high-capacity fiber connections are used for

transport closer to the core network and in the core network, where the network needs to handle aggregated traffic from many BSs.

The deployed backhaul technology today has large regional variations, but on a global scale, wireless microwave technology has historically been a dominating media for a long time. Over the last 10 years there has however been a large increase in fiber deployments attributed to, e.g., geopolitical decisions and major governmental investments. Over the same time, the use of copper as a media has reduced a lot due to increasing demands on capacity and lower maintenance. Going forward there are thus two dominating backhaul media – microwave and fiber. Historical and predicted global backhaul media distribution can be found in [4].

Fiber offers reliable high-capacity transport with demonstrated Tbps rates. However, the deployment of fiber requires a noteworthy initial investment for trenching and installation, which could take a considerable installation time, and even might not be possible/allowed in, certain areas where trenching is not an option.

Wireless backhauling using microwave represents a competitive alternative to fiber since it today provides 10's of Gbps in commercial deployments and even 100 Gbps has recently been demonstrated [5]. Microwave is a backhaul technology used by most mobile operators worldwide, and this trend is likely to continue. This is because microwave is a scalable and economical backhaul option that can meet the increasing requirements of 5G systems. A key advantage over fiber is that wireless backhauling comes with significantly lower cost and flexible/timely deployment (e.g., no digging, no intrusion or disruption of infrastructure, and possible to deploy in principle everywhere) [4], [6]. Today microwave backhauling operates in licensed point-to-point (PtP) spectrum, typically in the 4–70/80 GHz range. However, with the introduction of 5G in millimeter wave (mmWave) spectrum and with the foreseen need for even wider bandwidths for backhaul, microwave is currently being extended to even higher frequencies, above 100 GHz.

For the same reasons, and driven by network densification and access to wide bandwidth in mmWave spectrum, integrated access and backhaul (IAB) networks, where the operator can utilize part of the radio resources for wireless backhauling, has recently received considerable attention [7], [8]. The purpose of IAB is to provide flexible wireless backhauling using 3GPP new radio (NR) technology in international mobile telecommunications (IMT) bands, *providing not only backhaul but also the existing cellular services in the same node.* Thus, IAB serves as a complement to microwave PtP backhauling in dense urban and suburban deployments, while it comes at the expense of using IMT bands not only for access but also for backhaul traffic.

Wireless backhauling has been studied earlier in 3GPP in the scope of LTE Rel-10, also known as LTE relaying [9]. However, there have been only a handful of commercial LTE relay deployments, mainly because the existing LTE spectrum is very expensive to be used for backhauling, and also small-cell deployments did not reach the anticipated potential in the 4G timeline.

For 5G NR, IAB has been standardized in 3GPP Rel-16 and, as we detail later in the paper, standardization will continue in Rel-17. The main reason why NR IAB is expected to be more commercially successful than LTE relaying is that:

- The limited coverage of mmWave access creates a high demand for denser deployments, which, in turn, increases the need for backhauling.
- Also, the larger bandwidth available in mmWave spectrum provides more economically viable opportunity for wireless backhauling.
- Finally, MIMO, multi-beam systems, and multiple access, which are inherent features of NR, enable efficient backhauling of multiple radio BSs using the same equipment.

There have been several studies on the performance of IAB networks. For instance, cost-optimal node placement [10], resource allocation [11]–[14] and routing [11]–[17] are studied in the cases with different numbers of hops. Particularly, [10] provides an overview of multi-hop IAB techniques supported in the 3GPP rel-16 standard and discusses its design strategies. A joint node placement and resource allocation scheme maximizing the downlink sum rate is developed in [18]. Also, [19] uses simulated annealing algorithms for joint scheduling and power allocation. The maximum extended coverage area of a single fiber site using multi-hop relaying is investigated in [20], and [21], [22] perform end-to-end simulations to check the feasibility/challenges of mmWave-based IAB networks. Also, [23] provides useful insights for IAB deployments, especially, related to network densification and multi-hop topology, as it simulates a multi-hop mmWave pico-cell network, and evaluates the user throughput. The potential of using IAB in a fixed wireless access use-case is evaluated in [24]. The impact of dynamic time division duplex (TDD)-based resource allocation on the throughput of IAB networks, how its performance compares with static TDD and FDD (F: frequency), is discussed in [25], [26]. Moreover, [27]–[29] characterize the coverage probability of IAB-enabled mmWave heterogeneous networks via infinite Poisson point processes (PPPs). Precoder design and power allocation, to maximize the network sum rate, is considered in [30]. Finally, [31] investigates the usefulness of IAB in unmanned aerial vehicle (UAV)-based communications, and [32] develops a reinforcement learning-based resource allocation scheme in such networks.

In this article, we study the performance of IAB networks from different perspectives. We start by summarizing the most recent 3GPP discussions in Rel-16 as well as the upcoming ones in Rel-17, and highlight the main IAB-specific features on different protocol layers. Then, concentrating on mmWave-based communications, we analyze the performance of IAB networks, and compare their

performance with those achieved with hybrid IAB/fiber-connected networks. Here, the results are presented for the cases with an FHPPP (FH: finite homogeneous)-based stochastic geometry model, e.g., [27], [33], i.e., a PPP which depends on a constant density, with random distributions of the IAB nodes as well as the user equipments (UEs) in a finite region. Particularly, we study the network service coverage probability, defined as the probability of the event that the UEs' minimum data rate requirements are satisfied.

One of the key differences between fiber-connected and IAB networks is that, the backhaul link in IAB networks may, like any wireless link, be impacted by various weather effects and deployment conditions such as rain, blockage, antenna heights, and tree foliage. For this reason, we evaluate the impacts of these aspects. The results are presented for both suburban and urban areas, with the main focus on dense deployments, since that is the most interesting scenario for IAB.

In summary, the paper presents an easy-to-follow description of the most recent 3GPP agreements on IAB, gives cost/performance comparisons between the IAB and fiber-connected networks, and verifies the robustness of the network to different environmental effects, which makes the paper completely different from the related literature.

As we demonstrate, along with microwave backhauling, IAB is a cost-effective complement of fiber, especially in dense metropolitan areas. Moreover, independently of the cost, IAB is an appropriate tool in a number of use-cases of interest in 5G. Finally, as we show, while the coverage rate of the IAB network is slightly affected by heavy rainfall in suburban areas, for a broad range of parameter settings and different environments, the blockage and the rain are not problematic for IAB networks, in the sense that their impact on the coverage probability is negligible. High levels of tree foliage, however, may reduce the coverage probability of the network, especially in suburban areas.

The rest of the paper is organized as follows. Section II summarizes the key 3GPP discussions in Rel-16 and 17 on IAB. Section III describes the performance evaluation of IAB networks, compares their performance with those achieved in hybrid IAB/fiber-connected networks, and verifies the robustness of the IAB setup to different weather and deployment parameters. Finally, conclusions and a number of interesting open research problems that encourages researchers to contribute are provided in Section IV.

II. IAB IN 3GPP

NR IAB was introduced in 3GPP Rel-16. It provides functionality that allows for the use of the NR radio-access technology not only for the link between BSs and devices, sometimes referred to as the access link, but also for wireless backhaul links, see Figure 1.

Wireless backhauling, that is, the use of wireless technology for backhaul links, has been used for many years. However, this has then been mainly based on radio technologies different from those used for the access links.
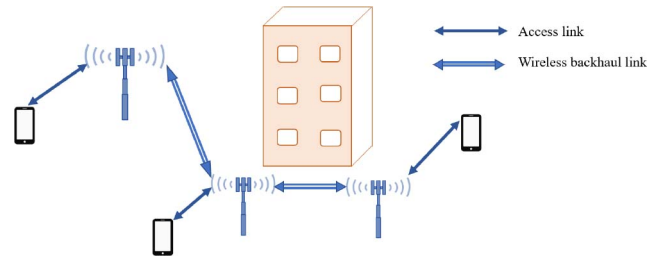

FIGURE 1. Integrated access and backhaul.

Additionally, wireless backhaul has typically been based on proprietary, i.e., non-standardized,[1] radio technology operating in mmWave spectrum above 10 GHz[2] and constrained to line-of-sight (LOS) propagation conditions.

However, along with massive amount of available spectrum due to the move to mmWave, there are at least two factors that now make it more relevant to consider an IAB solution, that is, reusing the standardized cellular technology, normally used by devices to access the network, also for wireless-backhaul links:

- With the emergence of 5G NR, the cellular technology is extending into the mmWave spectrum, a spectrum range that historically is used for wireless backhaul.
- With the emergence of small-cell deployments with BSs located, for example, on street level, there is a demand for a wireless-backhaul solution that allows for backhaul links to operate also under non-line-of-sight (NLOS) conditions, the kind of propagation scenarios for which the cellular radio-access technologies have been designed.

A. IAB ARCHITECTURE

The IAB standard that is being specified in 3GPP Rel-16 [35] is based on the split architecture introduced in 3GPP Rel-15, where a base station (gNB) is split into a centralized unit (CU), which terminates the Packet Data Convergence Protocol (PDCP) and the Radio Resource Control (RRC) protocol, and a distributed unit (DU) that terminates the lower layer protocols, i.e., Radio Link Control (RLC), Medium Access Control (MAC) and the physical layer [36]. The motivation for the CU/DU functional split is that all time-critical functionalities, e.g., scheduling, fast retransmission, segmentation etc., can be realized in the DU, i.e., close to the radio and the antenna, while it is possible to centralize and resource-pool the less time-critical radio functionalities in the CU. A specified interface (F1 interface) is used to convey both the control-plane (F1-C) and user-plane (F1-U) messages between the CU and DU. The CU/DU split is transparent to the UE, i.e., it does not impact UE functionality or protocol stack.

---

1. Some aspects of microwave backhauling are standardized, but there is significant room for proprietary solutions.
2. Traditional wireless backhaul operates also below 10 GHz, for example the longhaul links are typically at 6 GHz [34].
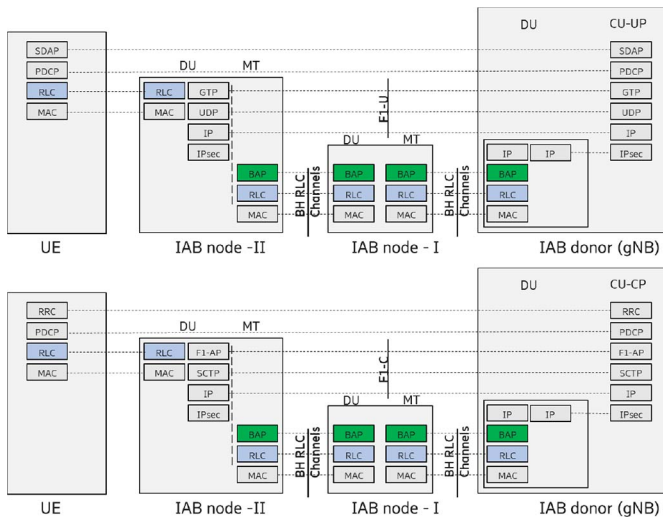
FIGURE 2. User plane and control plane protocol stack of a multi-hop IAB network according to 3GPP Rel-16.

Figure 2 shows the control and user plane protocol stack of a multi-hop IAB network according to 3GPP Rel-16. The IAB donor node is the node that is connected to the rest of the network in a conventional way (e.g., fiber or microwave) and serves the IAB nodes and other UEs that are directly connected to it. The IAB nodes have a mobile termination (MT) part and a DU part. The MT part is used to connect to a parent DU (which could be the donor DU or the DU part of another IAB node), while the DU part of an IAB node is used to serve UEs or the MT part of child IAB nodes.

In many respects, the MT part of an IAB node behaves like a UE in the sense that it communicates with the parent DU very much like a UE. On the other hand, from the UE point-of-view, the DU of an IAB node appears as a normal DU. This is necessary to preserve backwards compatibility so that legacy (pre Rel-16) NR UEs could also access the network via an IAB node.

As in legacy CU/DU split, for the user plane, the service data adaptation protocol (SDAP) and PDCP are terminated at the UE and the user plane part of the CU (CU-UP), and the corresponding packets are transported over an F1-U interface (basically, a set of GTP tunnels for each bearer) between the CU-UP and the DU part of the IAB node serving the UE (known as access IAB node). Similarly, for the control plane, the RRC and PDCP are terminated at the UE and the CU-CP, and the corresponding packets are transported over an F1-C interface, which is realized via a set of stream control transport protocol (SCTP) associations/streams between the CU-UP and the DU part of the access IAB node. The IAB-MTs can employ all the functionalities available to UEs such as carrier aggregation and dual connectivity to multiple parent nodes. The IAB nodes's protocol/architecture is transparent to the UE, i.e., UEs cannot differentiate between normal gNBs and IAB nodes.

In Rel-16, only a directed acyclic graph (DAG) multi-hop topology was supported, i.e., no mesh-based connectivity.

Also, only decode-and-forward relaying was considered, where the signal is decoded in each hop and, with a successful decoding, it is re-encoded and transferred to the next hop. Compared to other relaying techniques, this gives the best E2E performance in the multi-hop setup and make it possible to scale the network to the cases with different numbers of hops, especially, due to its full processing capability. The IAB nodes are interconnected with each other at layer 2 level and a hop-by-hop RLC is employed. This provides a better performance than having an end-to-end (E2E) RLC between the donor and the UE because retransmissions, if any, are required only over the affected hop, rather than between the UE and the donor, leading to faster and most efficient recovery to transmission failures. Hop-by-hop RLC also leads to lower buffering requirements at the end points. With regard to security, no hop-by-hop security is needed between the IAB nodes since the PDCP at the UE and CU ensure E2E encryption and integrity protection (optional for user plane).

1) ON BACKHAUL ADAPTATION PROTOCOL

A new protocol known as backhaul adaptation protocol (BAP) is specified that is responsible for the forwarding of packets in the intermediate hops between the donor DU and the access IAB node [37]. Each IAB node is configured with a unique BAP ID by the donor node. For downlink (DL) packets, the donor DU inserts a BAP routing ID on the packets it is forwarding to the next hop, which is the BAP ID of the access IAB node serving the UE and a path identifier, in case there are several possible paths to reach the access IAB node. Similarly, for uplink (UL) packets, the access IAB node inserts the UL BAP routing ID, which is the BAP ID of the donor DU and a path identifier, in case there are several possible paths to reach the DU. Each IAB node is configured with UL and DL routing tables, which indicates to which child node (in the case of DL) or parent node (in the case of UL) the packet should be forwarded. When an access IAB node receives a packet that is destined to it, the packet will be forwarded to higher layers and processed the same way a normal DU processes incoming F1-U or F1-C packets.

In addition to forwarding packets to a child or parent node, the BAP protocol also performs the mapping between ingress and egress backhaul RLC channels, to ensure that the packets are treated with the proper quality of service (QoS) requirements. Similar to RLC channels between a DU and a UE, the backhaul RLC channels can be configured with different QoS parameters such as priority and guaranteed bit rates. For bearers that have very strict QoS requirements, a 1:1 mapping could be used, where there is a dedicated backhaul RLC channel on each hop. Otherwise, an 1:N mapping can be employed where packets belonging to several bearers could be transported/multiplexed over a given backhaul RLC channel. Similar to the routing table, the IAB nodes are configured with a mapping configuration to determine which egress backhaul RLC channel a packet should be forwarded
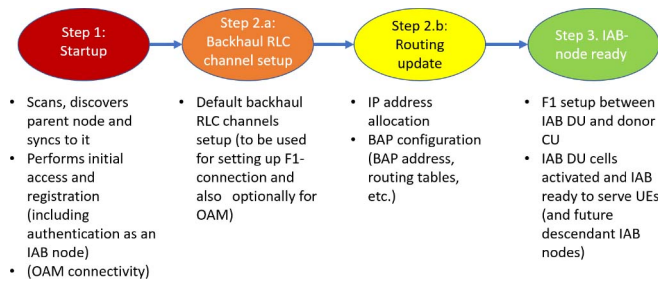
FIGURE 3. Schematic diagram of the IAB integration procedure in 3GPP Rel-16.

to once the next child/parent node has been identified via the routing table.

2) ON INTEGRATION PROCEDURE

Before becoming fully operational, the IAB node performs the IAB integration procedure, which is illustrated in Fig. 3 (interested reader is referred to [38] for the details). In the first step (startup), the IAB node performs an RRC connection establishment, like a normal UE, using its MT functionality. Once the connection is set up, it indicates to the network that it is an IAB node, which the network verifies/authenticates. Connectivity to the Operation and Maintenance (OAM) part of the network could also be performed at this phase to update configurations.

In the second step, the required/default backhaul RLC channel(s) are established, to enable the bootstrapping process where the DU part of the IAB node establishes the F1 connection with the donor as well as enable OAM connectivity (if not performed during the first step). A routing update is also made, which includes several sub-procedures such as IP address allocation for the IAB node and the (re)configuration of the BAP sub-layer at the IAB node and possibly all ancestor IAB nodes (BAP routing identifier(s) for downstream/upstream directions, routing table updates, etc.).

In the last step, the DU part of the IAB node can initiate an F1 connection request towards the donor CU, using its newly allocated IP address. After the F1 connection is set up, the IAB node can start serving UEs like a normal DU. Reconfigurations can be made anytime after this step, on a need basis, to update the backhaul RLC channels, routing tables, bearer mapping, etc.

B. SPECTRUM FOR IAB

As already mentioned, although IAB supports the full range of NR spectrum, for several reasons the mmWave spectrum is most relevant for IAB:

- The potentially large amount of mmWave spectrum makes it more justifiable to use part of the spectrum resources for wireless backhaul.
- Massive beamforming enabled at higher frequencies is especially beneficial for the wireless-backhaul scenario with stationary nodes at both ends of the radio link.

Higher-frequency spectrum is mainly organized as unpaired spectrum. Thus, operation in unpaired spectrum

has been the main focus for the 3GPP discussions on IAB. IAB supports both outband and inband backhauling:

- Outband backhauling: The wireless backhaul links operate in a different frequency band, compared to the access links.
- Inband backhauling: The wireless backhaul links operate in the same frequency band, as the access links.

C. THE IAB RADIO LINK

In most respects, the backhaul link, between a parent-node DU and a corresponding child IAB-node MT operates as a conventional network-to-device link. Consequently, the IAB-related extensions to the NR physical, MAC, and RLC layers are relatively limited and primarily deal with the need to coordinate the IAB-node MT and DUs for the case of inband operation when simultaneous DU and MT operation is not possible.

Similar to UEs, a time-domain resource of an IAB-node MT can be configured/indicated as:

- Downlink (DL): The resource will only be used by the parent node in the DL direction.
- Uplink (UL): The resource will only be used by the parent node in the UL direction.
- Flexible (F). The resource may be used in both the DL and UL directions with the instantaneous transmission direction determined by the parent-node scheduler.

Similarly, the time-domain resources of the DU part of an IAB node can be configured as:

- Downlink (DL): The DU can only use the resource in the DL direction.
- Uplink (UL): The DU can only use the resource in the UL direction.
- Flexible (F): The DU can use the resource in both the DL and UL directions.

In parallel to the DL/UL/F configuration, DU time-domain resources could be configured as hard or soft. In case of a hard configuration, the DU of a node can use the resource without having to consider the impact on its MTs ability to transmit/receive according to its configuration and scheduling. In practice this means that, if a certain DU time-domain resource is configured as hard, the parent node must assume that the IAB-node MT may not be able to receive/transmit. Consequently, the parent node should not schedule transmissions to/from the MT in this resource.

In contrast, in case of a DU time-domain resource configured as soft, the DU can use the resource if and only if this does not impact the MTs ability to transmit/receive according to its configuration and scheduling. This means that the parent node can schedule a DL transmission to the MT in the corresponding MT resource and assume that the MT is able to receive the transmission. Similarly, the parent node can schedule MT UL transmission in the resource and assume that the MT can carry out the transmission.

The possibility to configure soft DU resources allows for more dynamic resource utilization. Take, as an example, a

soft DU resource corresponding to an MT resource configured as UL. If the MT does not have a scheduling grant for that resource, the IAB node knows that the MT will not have to transmit within the resource. Consequently, the DU can dynamically use the resource, for example, for DL transmission, even if the IAB node is not capable of simultaneous DU and MT transmission.

The possibility to configure soft DU resources also gives an IAB node the chance to benefit from being able to perform simultaneous DU and MT operation. Whether or not a specific IAB node is capable of simultaneous DU and MT operation may depend on the IAB-node implementation and may also depend on the exact deployment scenario. Thus, an IAB node designed or deployed so that it can support simultaneous DU and MT operation can use a soft DU resource without the parent node even knowing about it.

These situations, when an IAB node, by itself, can conclude that it can use a soft DU resource has, in the 3GPP discussions, been referred to as implicit indication of availability of soft DU resources. The parent node can also provide an explicit indication of availability of a soft DU resource by means of layer-1 signaling.

Finally, it should be noted that, along with resource multiplexing which has been the main topic of discussions in RAN1, the over-the-air (OTA) timing alignment, the random access channel (RACH) as well as the extensions of SSBs for inter-IAB-node discovery and measurements have been discussed in 3GPP. However, due to space limits, we do not cover these topics, and the interested reader can find the final agreements in [39]. Moreover, while we concentrated mostly on RAN1 and RAN2 discussions, the main discussions/agreements in RAN3 and RAN4 can be found in [40]–[41] and [42], respectively (also see [10]).

D. IAB IN REL-17

The physical-layer part of the IAB Rel-16 specifications was finalized at the end of 2019 and the remaining parts (higher-layer protocols and architecture) are expected to be finalized in June 2020. Further enhancements to IAB will then be carried out within 3GPP Rel-17, with expected start in August 2020 [43]. The Rel-17 work aims to improve on various aspects such as robustness, degree of load-balancing, spectral efficiency, multi-hop latency and end-to-end performance. More specifically, the following is planned to be covered:

- Enhancements to the resource multiplexing between child and parent links of an IAB node, including:
  - Enhanced support of simultaneous operation (transmission and/or reception) of IAB-node's child and parent links, including enhancements such as new DU/MT timing relations, DL/UL power control and cross link interference mitigation.
  - Support for dual-connectivity scenarios for topology redundancy for improved robustness and load balancing.

- Enhancements in scheduling, flow and congestion control to improve end-to-end performance, fairness, and spectral efficiency.
- Introduction of efficient inter-donor IAB-node migration, increasing the robustness of IAB networks allowing for more refined load-balancing and topology management.
- Reduction of service interruption time caused by IAB-node migration and backhaul RLF recovery improves network performance, allows network deployments to undergo more frequent topology changes, and provides stable backhaul performance.

Finally, it should be mentioned that in 3GPP RAN4 a number of simulations have been performed to evaluate the feasibility/efficiency of IAB networks, e.g., [44]. There, it has been mainly concentrated on defining RF requirements for both backhaul and access links of an IAB-node including requirements for their co-existence, and evaluate the performance in different possible scheduling scenarios of the DU and MT. In Section III, we mainly concentrate on the comparison between the performance of IAB and fiber networks as well as studying the robustness of IAB networks to different environmental effects using a novel stochastic geometry modeling for mmWave networks and 3D maps topology information. Such results provide insights about if the IAB performance expectations will be met in urban and suburban areas.

III. PERFORMANCE EVALUATION

This section studies the service coverage rate of IAB networks with various parameterizations, and compares the performance with those achieved by (partially) fiber-connected networks. First, we present the system model, including the channel model, the considered UE association rule as well as the rain, the blockage and the tree foliage models, which are followed by the simulation results.

A. SYSTEM MODEL

As shown in Fig. 4, consider an outdoor two tier heterogeneous network (HetNet), i.e., a two-hop IAB network, with multiple MBSs (M: macro), SBSs (S: small) and UEs. This is motivated by different evaluations, e.g., [27]–[30], where, although the standardization does not limit the number of hops, increasing the number of hops may lead to backhaul traffic aggregation. In an IAB deployment, both the MBSs and the SBSs use wireless connections for both access and backhaul. Also, only the MBSs are fiber-connected while the SBSs receive data from the MBSs wirelessly by using IAB. That is, following the 3GPP definitions (see Section II), the MBSs and the SBSs can be considered as the donor and the child IABs, respectively. Therefore, throughout the section, we may use the terminologies MBS/SBS and donor IAB/IAB interchangeably. Considering an inband operation, the bandwidth is shared among access and backhaul links of the IAB nodes such that the network service coverage rate
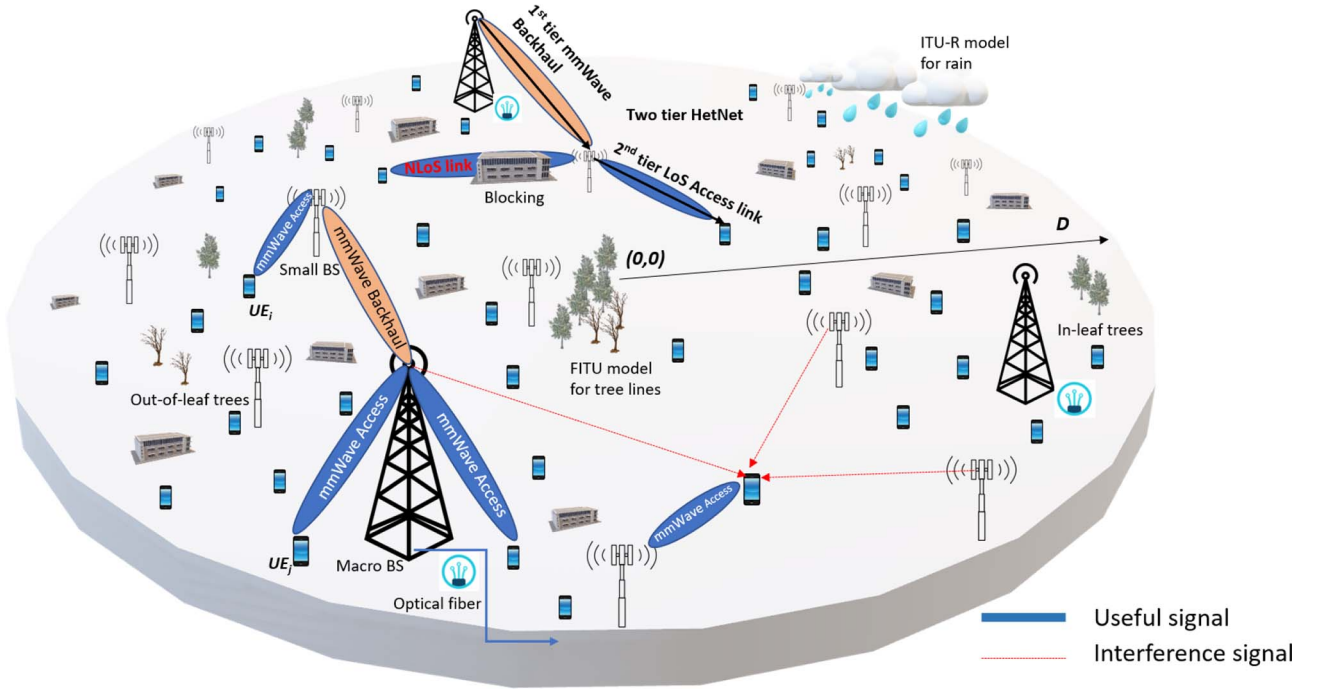
FIGURE 4. Schematic of the IAB system model.

TABLE 1. The definition of the parameters.

Parameter	Definition	Parameter	Definition
ϕ_M	FHPPP of the MBSs	ϕ_U	FHPPP of the UEs
ϕ_S	FHPPP of the SBSs	λ_U	UE density
ϕ_B	FHPPP of the blocking walls	θ	Orientation of blocking wall
ϕ_T	FHPPP of the tree lines	l_{hop}	Average hop length
λ_M	MBSs density	λ_S	SBSs density
H	Homogeneous Poisson Process	λ_B	Blocking wall density
l_B	Blocking wall length	ρ	Service coverage probability
A	Circular disk	D	Radius of the disk
P_t	Transmission power	P_r	Received power
h	Fading coeficient	G	Antenna gain
$L_{(1m)}$	Reference path loss at 1 meter distance	L	Propagation path loss
x	Location of the node	r	Propagation distance between the nodes
α	Path loss exponent	N	Number of UEs connected
f_c	Carrier frequency	φ	Angle between the BS and UE
θ_{HPBW}	Half power beamwidth of the antenna	G_0	Maximum gain of directional antenna
$g(\varphi)$	Side lobe gain	R_{th}	Minimum data rate threshold
x_c	Associated cell	R	Rain intensity
x_u	Connected UE at the location	i, j	Node index
F_T	Tree foliage	γ_R	Rainloss
d	Vegetation depth	W	Bandwidth of the DL
μ	Percentage of bandwidth resources on backhaul	l_T	Tree line length
λ_T	Tree blocking density	v	SBS antenna height

is maximized. For simplicity, the MBSs and the SBSs are assumed to have constant power over the spectrum of the system and are all active throughout the analysis.[3]

1) SPATIAL MODEL

Table 1 summarizes the parameters used in the analysis. We model the IAB network by an FHPPP, e.g., [33], [45],

---

3. Developing adaptive power allocation schemes for IAB networks is an interesting open research topic.

which suits well to model a random number of nodes in a finite region. Particularly, FHPPPs ϕ_M and ϕ_S with densities λ_M and λ_S, respectively, are used to model the spatial distributions of the MBSs and the SBSs, respectively.

The MBSs' FHPPP is given by $\phi_M = H \cap A$, where H with density λ_M is an HPPP (H: homogeneous) and $A \subset \mathbb{R}^2$ is a finite region. For simplicity and without loss of generality, we let A be a circular disk with radius D. However, the study is generic and can be applied on arbitrary regions A. The SBSs and the UEs are also located within the same A

in accordance with two other FHPPPs ϕ_S and ϕ_U having densities λ_S and λ_U, respectively, which are all mutually independant.

We study the system performance for two blocking conditions. First, we use the well-known germ grain model [46, Ch. 14], which provides accurate results compared to stochastic models that assume the blocking in different links to be independant. Moreover, the germ grain model fits well for environments with large obstacles as it takes the obstacles induced blocking correlation into account. The model is an FHPPP, i.e., the blockages are distributed according to the FHPPP ϕ_B distributed in the same area A with density λ_B. This is a 2D model where all blockings are assumed to be walls of length l_B and orientation θ, which is an independantly and identically distributed (IID) uniform random variable in $[0, 2\pi]$. The walls are distributed in random locations uniformly as of the FHPPP.

With the 2D channel model, the elevation of the blocking and the BSs or the terrain information of the land are not taken into account. For this reason, in Section III-C4, we demonstrate the system performance for an example 3D usecase. Particularly, we distribute the same spatial arrangement of the MBSs, the SBSs and the UEs with their respective nodes heights on top of map data with real world blocking terrain using OpenStreetMap 3D environment. That is, while different MBS and SBS nodes are distributed randomly based on their corresponding FHPPPs, they are placed, on different heights, and the blockages are determined based on the map information. This enables us to evaluate the effect of the nodes and blocking heights on the service coverage probability.

2) CHANNEL MODEL

We consider an inband communication setup, where both the access and backhaul links operate in the same mmWave spectrum band. Following the state-of-the-art mmWave channel model, e.g., [45], the received power at each node can be expressed as

$$P_r = P_t h_{t,r} G_{t,r} L_{(1m)} L_{t,r} \|x_t - x_r\|^{-1} F_{t,r} \gamma_{t,r}. \quad (1)$$

Here, P_t denotes the transmit power in each link, and $h_{t,r}$ represents the independant small-scale fading for each link. The small-scale fading is modelled as a normalized Rayleigh random variable in our analysis. Then, $G_{t,r}$ represents the combined antenna gain of the transmitter and the receiver of the link, $L_{t,r}$ which is a function of the distance between x_t and x_r, denotes the path loss due to propagation, and $L_{(1m)}$ is the reference path loss at 1 meter distance. The tree foliage loss is denoted by $F_{t,r}$ while $\gamma_{t,r}$ represents the rain loss between the transmitter and the receiver of the link in linear scale. The total path loss, in dB, is characterized according to the 5GCM UMa close-in model described in [47]. The path loss is given by

$$\kappa = 32.4 + 10 \log_{10}(r)^{\alpha} + 20 \log_{10}(f_c), \quad (2)$$

where f_c is the carrier frequency, r is the propagation distance between the nodes, and α is the path loss exponent. Depending on the blockage, LOS and NLOS links are affected by different path loss exponents. The propagation loss of the path loss model is given by

$$L_{t,r} = \begin{cases} r^{\alpha_L}, & \text{if LoS,} \\ r^{\alpha_N}, & \text{if NLoS,} \end{cases} \quad (3)$$

where α_L and α_N denote path loss exponents for the LOS and NLOS scenarios, respectively. In 5G, large antenna arrays with directional beamforming are used to mitigate the propagation losses. We model the beam pattern as a sectored-pattern antenna array and thus the antenna gain between two nodes can be expressed by

$$G_{i,j}(\varphi) = \begin{cases} G_0 & \frac{-\theta_{HPBW}}{2} \leq \varphi \leq \frac{\theta_{HPBW}}{2} \\ g(\varphi) & \text{otherwise.} \end{cases} \quad (4)$$

Here, i, j are the indices of the considered transmit and receive nodes, and φ is the angle between them in the considered link. Also, θ_{HPBW} is the half power beamwidth of the antenna, and G_0 is the directional antenna's maximum gain while $g(\varphi)$ is the side lobe gain. Also, we let the UE antenna gain to be 0 dB. This is in harmony with, e.g., [27], [29], [48], and because the UE has an omni-directional radiation pattern. For discussions on how the antenna gain is affected by the antenna array properties, see, e.g., [45].

We assume that we have high beamforming capability in the IAB-IAB backhaul links. Consequently, we ignore the interference in the backhaul links and assume them to be noise-limited. Also, the inter-UE interferences are neglected due to the low power of the devices and with the assumption of sufficient isolation [24]. On the other hand, as illustrated in Fig. 4, the interference model focuses on the aggregated interference on the access links, due to the neighbouring interferers, which for UE u is given by

$$I_u = \sum_{i,j \in \phi_{i,j} \setminus \{x_c\}} P_j h_{i,j} G_{i,j} L_{(1m)} L_{x_i,x_j} \|x_i - x_j\|^{-1}. \quad (5)$$

Here, i and j represents all BSs except for the associated cell x_c which can either be an MBS or an SBS.

3) RAIN AND TREE FOLIAGE MODEL

With the need of understanding the performance of IAB networks in rainy conditions, we use the ITU-R Rec 8.38-3 rain model [49] to entail the rain effect on the links. This is an appropriate model used to methodically determine the amount of rain attenuation on radio links. The model is widely used in all regions of the world, for the frequency range from 1 GHz to 1000 GHz with no rain rate obligation. The model describes the rain loss as

$$\gamma_R = kR^{\beta}, \quad (6)$$

where γ_R is the rain loss in dB/km, and R is the rain intensity in mm/hr. Moreover, k and β are coefficients that are precalculated depending on the carrier frequency. Table II shows the coefficients for horizontal and vertical losses at

TABLE 2. Coefficients for ITU-R model. Here, β_h, k_h are the horizontal polarization coefficients and β_v, k_v denote the vertical polarization coefficients [49].

Frequency (GHz)	β_h	β_v	k_h	k_v
28	0.9679	0.9277	0.2051	0.1964

rainy conditions in 28 GHz on which we concentrate in the simulations.

Finally, FHPPP ϕ_T with density λ_T is used to spatially distribute the tree lines of length l_T [50]. We use the Fitted International Telecommunication Union-Radio (FITU-R) tree foliage model [51, Ch. 7] to model the effect of the trees on the received signal power. This is an appropriate model for the cases with frequency dependancy and with non-uniform vegetation. The model is suitable for the mmWave frequencies from 10 to 40 GHz and has been derived by further developing the ITU-R vegetation model. In this way, considering two, namely, *in-leaf* and *out-of-leaf*, vegetation states, the tree foliage in dB is obtained by

$$F_T = \begin{cases} 0.39 f_c^{0.39} d^{0.25}, & \text{in-leaf} \\ 0.37 f_c^{0.18} d^{0.59}, & \text{out-of-leaf}, \end{cases} \quad (7)$$

where f_c is the carrier frequency expressed in MHz and d is the vegetation depth in meter.

B. ASSOCIATION AND ALLOCATION STRATEGY

In our setup, the UE can be served by either an MBS or an SBS following open access strategy and based on the maximum average received power rule. Also, in harmony with 3GPP, we do not take joint transmission into account, i.e., each UE can be connected to only one MBS or SBS. In this way, the association rule for UE u suffices

$$\sum_{\forall j} u_j = 1, \ \forall_u \in U, u_i \cdot u_j = 0, \forall j \neq i, \quad (8)$$

where $u_j \in \{0, 1\}$ is a binary variable indicating the association with 1 and 0 denoting the unassociated cell. For the access links of the UEs, we have

$$u_j = \begin{cases} 1 & \text{if } P_i G_{z,x} h_{z,x} L_{(1m)} L_{z,x}(\|\mathbf{z} - \mathbf{x}\|)^{-1} \\ & \geq P_j G_j h_{z,y} L_{(1m)} L_{z,y}(\|\mathbf{z} - \mathbf{y}\|)^{-1}, \\ & \forall \ \mathbf{y} \in \phi_j | \mathbf{x} \in \phi_i, i, j \in \{m, s\} \\ 0, & \text{otherwise.} \end{cases} \quad (9)$$

As in (9) for each UE u, the association binary variable u_j becomes 1 for the cell giving the maximum received power at the UE, while for all other cells it is 0 since the UE can only be connected to one IAB node.

Because the IAB nodes, i.e., both the MBSs and the SBSs, are equipped with large antenna arrays and can beamform towards the required direction, the antenna gain over the backhaul links can be assumed to be the same, and back-haul link association can be well determined based on the minimum path loss rule, i.e., by

$$x_{b,m} = \begin{cases} 1 & \text{if } L_{b_m}(\|\mathbf{z} - \mathbf{x}\|)^{-1} \geq L_{b_m}(\|\mathbf{z} - \mathbf{y}\|)^{-1}, \\ & \forall \ \mathbf{y} \in \phi_m | \mathbf{x} \in \phi_m, \\ 0, & \text{otherwise} \end{cases} \quad (10)$$

(For the effect of interference in the backhaul links, see Fig. 6). For resource allocation, on the other hand, the mmWave spectrum available is partitioned into the access and backhaul links such that

$$\begin{cases} W_{\text{Backhaul}} = \mu W, \\ W_{\text{Access}} = (1 - \mu)W, \end{cases} \quad (11)$$

with $\mu \in [0, 1]$ being the percentage of bandwidth resources on backhauling. Also, W_{backhaul} and W_{access} denote the back-haul and the access bandwidths, respectively, while total bandwidth is W. The bandwidth allocated for each SBS, i.e., child IAB, by the fiber-connected MBS, i.e., IAB donor, is proportional to its load and the number of UEs in the access link. The resource allocation is determined based on the instantaneous load in which each SBS informs its current load to the associated MBS each time. Thus, the backhaul-related bandwidth for the j-th IAB node is given by

$$W_{\text{backhaul},j} = \frac{\mu W N_j}{\sum_{\forall j} N_j}, \forall j, \quad (12)$$

where N_j denotes the number of UEs connected to the j-th IAB node. Therefore, the bandwidth allocated to the j-th IAB node is proportional to the ratio between its load, and the total load of its connected IAB donor. Meanwhile, the access spectrum is equally shared among the connected UEs at the IAB node according to

$$W_{\text{access},u} = \frac{(1 - \mu)W}{\sum_{\forall u} N_{j,u}}, \forall u, \quad (13)$$

where u represents the UEs, and j represents each IAB node. Also, $N_{j,u}$ denotes the users connected to the j-th IAB node of which UE u is connected. The signal-to-interference-plus-noise ratio (SINR) values are obtained in accordance with (5) by

$$\text{SINR} = P_r/(I_u + N_0), \quad (14)$$

where N_0 is the noise power. Then, considering sufficiently long codewords, which is an acceptable assumption in IAB networks, the rates experienced by the UEs in access links can be expressed by

$$R_u = \begin{cases} \frac{(1-\mu)W}{N_m} \log(1 + \text{SINR}(x_u)), & \text{if } \mathbf{x}_c \in \phi_m, \\ \min\Big(\frac{(1-\mu)W}{\sum_{\forall u} N_{j,u}} \log(1 + \text{SINR}(x_u)), \\ \quad \frac{\mu W N_j}{\sum_{\forall j} N_j} \log(1 + \text{SINR}(x_b))\Big), & \text{if } \mathbf{x}_c \in \phi_s, \end{cases} \quad (15)$$

and the backhaul rate is given by

$$R_b = \frac{\mu W N_j}{\sum_{\forall j} N_j} \log(1 + \text{SINR}(x_b)). \quad (16)$$

Here, m represents the associated MBS and s denotes the SBS. Based on the association cell, there are two cases for the rate of the connected UEs, x_u at the location. First, is the case in which the UEs are associated to the MBSs, as denoted by $x_c \in \phi_m$ in (15). Since the MBSs, i.e., IAB donor nodes, have fiber backhaul connection, the rate will depend on the access bandwidth available at the UE. In

TABLE 3. Simulation parameters.

| Parameters	Value
Carrier frequency	28 GHz
Minimum data rate threshold	100 Mbps
Bandwidth	1 GHz
IAB node and UE density	{MBS, SBS, UE} = (8, 100, 500) /km^2
Blocking	{Density, Length} = (500 /km^2, 5 m)
Path loss exponents	{LoS, NLoS} = (2, 3)
Main lobe antenna gains	{MBS, SBS, UE} = (24, 24, 0) dBi
Side lobe antenna gains	{MBS, SBS, UE} = (-2, -2, 0) dBi
Half power beamwidth	{azimuthal, elevation} = (60, 25)
Noise power	5 dB
In-leaf percentage	20%
Tree depth	5 m
Antenna heights	{MBS, SBS, UE} = (25,10,1) m

FIGURE 5. Density of the IAB nodes sufficing the performance of fiber-backhauled network, in terms of service coverage probability. The parameters are set to $\lambda_B = 500$ km^{-2}, no rain, $R_{th} = 100$ Mbps, and P_{MBS}, P_{SBS}, $P_{UE} = (40, 24, 0)$ dBm.

the second case, the UEs are connected to the SBSs, as denoted by $x_c \in \phi_s$ in (15). Here, the SBSs have shared backhaul bandwidth from the IAB donor nodes, i.e., MBSs, and thus the UEs data rates depend on the backhaul rate of the connected SBS as well. Thus, in this case the UE is bounded to get the minimum between backhaul and access rate.

C. SIMULATION RESULTS AND DISCUSSIONS

The simulation results are divided into three parts in which 1) we compare IAB, hybrid IAB/fiber-connected, and fiber-connected networks, 2) verify the robustness of IAB networks, and 3) study the system performance in an example of 3D network deployment. Note that the 2D model is considered mainly to limit the simulation complexity. However, for different cases, the same qualitative conclusions as those presented in the 2D model hold in the 3D model as well. The general system parameters are summarized in Table 3 and, for each figure, the specific parameters are given in the figure caption. The network is deployed in a disk of radius of $D = 1$ km, where the rain occurrence, the blockage, and the vegetation distributions are also probable according to the statistical models described in Section III-A. In all figures, except for Figs. 8 and 9 which study the system performance in both urban and suburban areas, we concentrate on dense areas as the most important point of interest in IAB networks. We assume that we have high beamforming capability in the IAB-IAB backhaul links. Consequently, in all figures except for Fig. 6, we ignore the interference in the backhaul links, in harmony with, e.g., [27]–[29]. In Fig. 6, however, we verify this assumption, and study the system performance in the cases where the interference is not ignored in the IAB-IAB links (More insights on mmWave interference in cellular networks are discussed in, e.g., [52], [53].)

Our metric of interest is the service coverage probability [54], defined as the fraction of the UEs which have instantaneous UE data rates higher than or equal to a threshold R_{th}. That is, using (15), the service coverage probability is given by

$$\rho = \Pr(R_U \geq R_{th}). \quad (17)$$
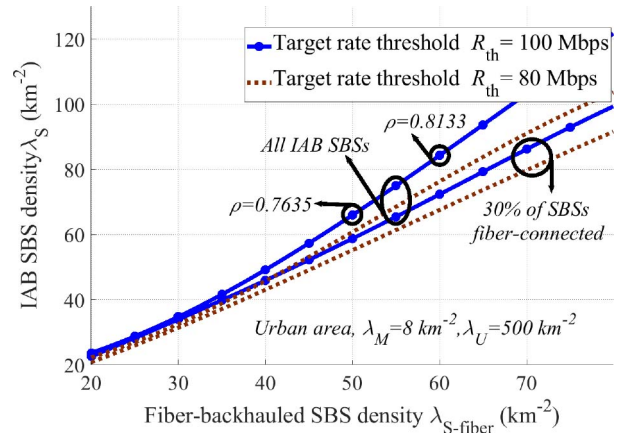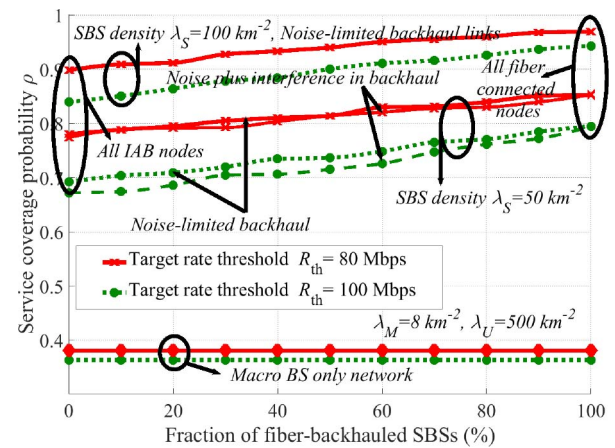
FIGURE 6. Service coverage probability as a function of the percentage of the fiber-backhauled SBSs for a dense network with $\lambda_B = 500$ km^{-2}, no rain and P_{MBS}, P_{SBS}, $P_{UE} = (40, 24, 0)$ dBm.

1) IAB VERSUS FIBER

In Figs. 5-6, we compare the coverage probability of the IAB networks with those obtained by the cases having (a fraction of) fiber-connected SBSs, as well as the cases with no SBS. Also, Fig. 6 verifies the effect of the interference in the backhaul links on the system performance. In these figures, different parameters, e.g., bandwidth allocation between the access and backhaul, have been optimized to maximize the coverage probability in each case. Note that, in practice and depending on the network topology, a number of SBSs may also be fiber-connected. For this reason, in Figs. 5-6, we also consider the cases with a fraction of SBSs having fiber connections. In such cases, we assume the fiber-connected SBSs to be randomly distributed, and adapt the association and allocation rules as well as the achievable rates, correspondingly.

Figure 5 demonstrates the required number of IAB nodes to guarantee the same coverage probability as in the cases with hybrid IAB/fiber-connected SBSs. Then, Fig. 6 shows

the network service coverage rate as a function of the fraction of fiber-connected SBSs, and compares the system performance with the cases having no SBS.

As demonstrated in Figs. 5-6, for a broad range of parameter settings, the same performance as in the fully fiber-connected networks can be achieved by the IAB network, with relatively small increment in the number of IAB nodes. As an example, consider the parameter settings of Fig. 5 and the UEs' target rate 100 Mbps. Then, a fully fiber-connected network with SBSs densities 50 and 60 km^{-2} corresponds, in terms of coverage probability, to an IAB network having densities $\lambda_S = 65$ km^{-2} and 85 km^{-2}, respectively, leading to coverage probabilities 0.76 and 0.81. Interestingly, with a 30% of SBSs having fiber connections, which is practically reasonable, these numbers are reduced to $\lambda_S = 70$ and 85 km^{-2}, i.e., only 16% and 21% increase in the required number of SBSs. Then, as the network density increases, the effect of the UEs target rate as well as the relative performance gap of the IAB and fiber-connected networks decrease (Fig. 6). Moreover, in harmony with intuitions and motivated by the high beamforming capability of the IAB nodes, the effect of the interference in the backhaul links is negligible, and the IAB-IAB links can be well assumed to be noise-limited (Fig. 6).

Here, it should be noted that our results, based on the FHPPP and random node drop, give a pessimistic performance of IAB networks. In practice, the network topology will be fairly well-planned, further reducing the gap between the performance of IAB and fiber-connected networks. Also, for simplicity and in order to mainly concentrated on the effect of environmental parameters, we considered the minimum path loss rule in the backhaul links. A smart network operator may, however, use load balancing techniques to avoid congestion in the network, e.g., [55], [56]. Finally, while we considered a fixed bandwidth split between the access and backhaul which limits the resource allocation/coordination complexity, an adaptive split between access and backhaul of different nodes would improve the network performance.

2) ON SOME PRACTICAL BENEFITS OF IAB

Using IAB with such a relatively small increment of the nodes reduces the network cost considerably.[4] This is because an SBS is much cheaper than fiber.[5] For example, and only to give an intuitive view, as reported in [57, Table 7], in an urban area the fiber cost is estimated to be in the range of 20000 GBP/km, while an SBS in 5G is estimated to cost around 2500 GBP per unit [58].[6] More importantly, internal evaluations at Ericsson indicates that,

for dense urban/suburban areas, even in the presence of dark fiber, the deployment of IAB networks is an opportunity to reduce the total cost of ownership (TCO) as well as the time-to-market. Especially, the same hardware can be used both for access and backhaul such that no extra and separate system is needed for backhaul.

Thus, although IAB may not support the same peak rate as fiber, IAB will be sufficient and a cost-effective solution for SBSs in dense networks, and with no digging,[7] traffic jam and/or infrastructure displacement.

Along with the cost reduction, IAB increases the network flexibility remarkably. With optical fiber, the access points, of different types, can be installed only in the places with fiber connection. Such a constraint is, however, relaxed in IAB networks, and the nodes can be installed in different places as long as they have fairly good connection to their parent nodes. These are the reasons that different operators have shown interest to implement IAB in 5G networks [61], and it is expected that IAB would be ultimately used in up to 10-20% of 5G sites, e.g., [62].

It is interesting to note that, regardless of the cost, IAB is an attractive solution for a number of use-cases:

- Street trenching and digging not only are expensive but also may destroy historical areas or displace trees. For such reasons, some cities may consider a moratorium on fiber trenching [59], and instead rely on wireless backhaul methods such as IAB and microwave backhaul.
- Fiber installation may take a long time, as it requires different permissions, labor work, etc. In such cases, IAB can establish new radio sites quickly. Thus, starting with IAB and, if/when needed, replacing it by fiber is expected to become a quite common setup.
- Low income zones of dense cities suffer from poor Internet connection. This is mainly because current fiber-based solutions are not economically viable, and the companies are not interested in fiber installation in such areas. Here, IAB is a low TCO solution to reduce the cost of Internet infrastructure.
- Public safety, and in general mission critical (MC), systems should be able to provide temporally on-demand coverage in all scenarios where the MC UEs are within terrestrial cellular network coverage or out of terrestrial cellular network coverage. In such cases, an IAB node, e.g., on a drone or a fire truck, can extend the coverage with high reliability and low latency.[8]

Finally, as expected and also emphasized in Fig. 6, as the number of UEs increases, MBSs alone can not support the UEs' QoS requirements, and indeed we need to densify the network with, e.g., using (IAB) nodes of different types.

---

4. It is reasonable to consider almost the same cost for an IAB node and a typical SBS.

5. Indeed, the exact cost of the fiber varies vastly in different regions, due to many factors including labour cost, etc. However, for different areas, fiber laying accounts to a significant fraction of the total network cost.

6. The price estimates are based on [57], and [58], and should not be considered as the cost estimations in Ericsson.

7. According to different reports, e.g., [59], [60], for fiber connection in metropolitan areas, a large portion (about 85%) of the total cost figure is tied to trenching and installation.

8. It should be noted that, within Rel-16 and 17, mobile IAB is not supported. Thus, with an IAB on, e.g., a drone, the node position should remain fixed during the data transmission.
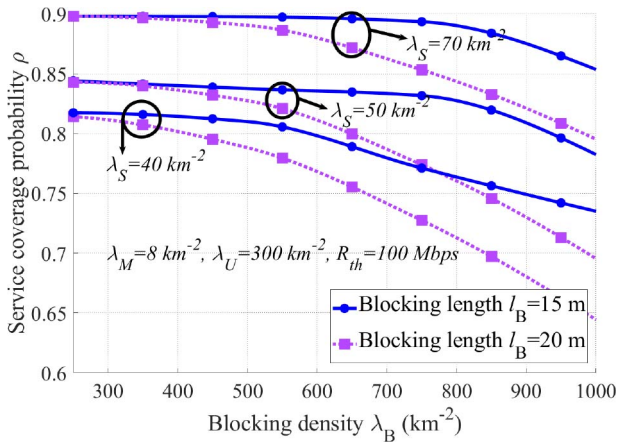
FIGURE 7. Service coverage probability of the IAB network as a function of the blocking density λ_B, with P_{MBS}, P_{SBS}, P_{UE} = (40, 24, 0) dBm, and no rain/tree foliage.
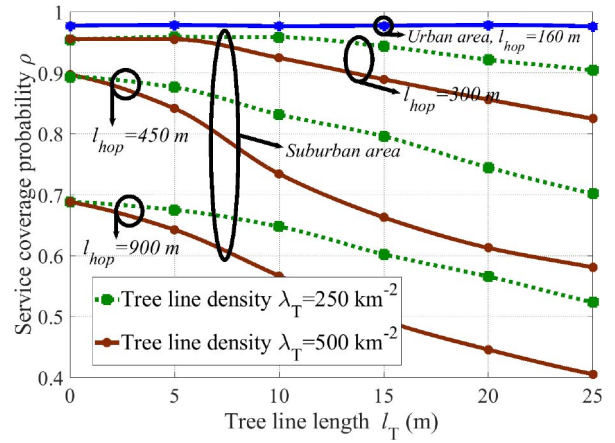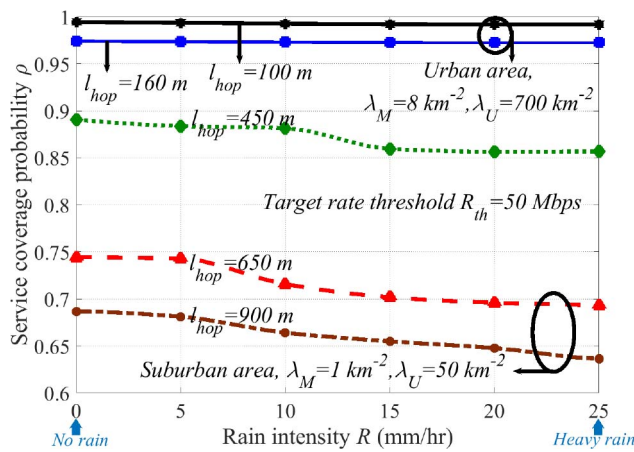

FIGURE 8. Service coverage probability of the IAB network as a function of the rain intensity in urban and suburban areas and for different average hop distances. The parameters are set to P_{MBS}, P_{SBS}, P_{UE} = (45, 33, 0) dBm, λ_B = 500 km^{-2} for urban area and no blocking for the suburban area. Average hop distances l_{hop} = 100, 160, 450, 650, 900 m correspond to SBS densities λ_S = 100, 50, 8, 5, 3 km^{-2}, respectively.

3) EFFECT OF RAIN, BLOCKING AND TREE FOLIAGE

As opposed to fiber-connected setups, an IAB network may be affected by blockage, rain and tree foliage, the effects of which are analyzed in Figs. 7-9, respectively. Particularly, considering the 2D FHPPP blockage model, Fig. 7 investigates the coverage probability for different blockage densities λ_B and walls lengths l_B (also, see Fig. 11 for the effect of blockage in a 3D model).

Although IAB is of particular interest in dense urban areas, it has the potential to be used in suburban areas as well. For this reason, in Figs. 8 and 9 we demonstrate the coverage probability as a function of, respectively, the rain intensity, R in (6), and the tree line length l_T in both urban and suburban areas. Here, the results are presented for the average hop distances l_{hop} = 100, 160, 450, 650, 900 m which correspond to SBSs densities λ_S = 100, 50, 8, 5 and 3 km^{-2}, respectively. For a suburban area, i.e., the

FIGURE 9. Service coverage probability of the IAB network, in both suburban and urban areas, as a function of the tree line length l_T with R_{th} = 50 Mbps, P_{MBS}, P_{SBS}, P_{UE} = (45, 33, 0) dBm, d = 5 m, in (7), and no rain. In the suburban area, we set λ_M = 1 km^{-2}, λ_U = 50 km^{-2} with no blockage, while for the urban area we set λ_M = 8 km^{-2}, λ_U = 700 km^{-2} with blockage having density λ_B = 500 km^{-2} and length l_B = 5 m. Average hop distances l_{hop} = 160, 300, 450, 900 m correspond to SBS densities λ_S = 50, 20, 8, 3 km^{-2}, respectively.
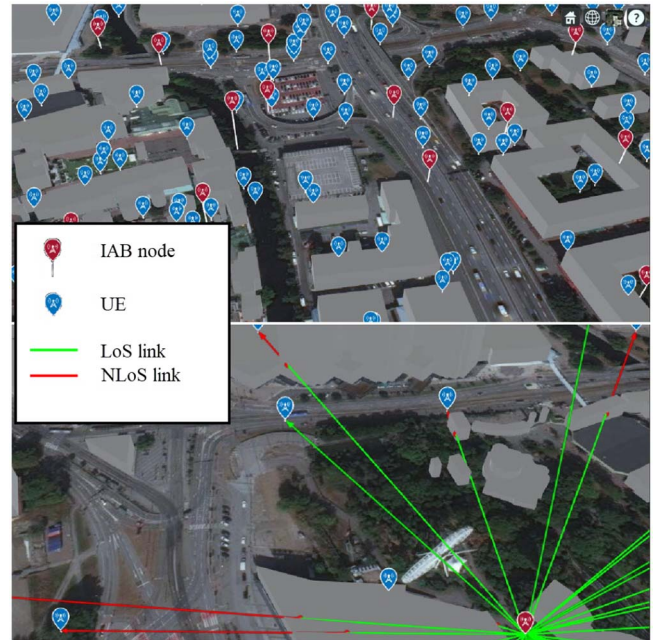

FIGURE 10. An example of the distribution of the IAB network in 3D space with OpenStreetMap.

cases with large average hop distance, we consider a single MBS, no blockage and UEs' density λ_U = 50 km^{-2}. On the other hand, for the cases with urban areas, i.e., low average hop distance, the blockage and the UEs, densities are set to λ_B = 500 km^{-2} and λ_U = 700 km^{-2}, respectively. According to Figs. 7-9, the following points can be concluded:

- Unless for low network densities, the coverage probability is not much affected by the blockage density/length (Fig. 7. also, see Fig. 11 for the effect of blockage in a 3D example use-case). This is intuitive because, as the network density increases, with high probability each

UE can be connected to an SBS with strong LOS signal component.

- Considering 28 GHz, rain will not be a problem for IAB, unless for the cases with very heavy rainfall in suburban areas (Fig. 8). Particularly, the system performance is robust to different rain intensities in suburban/urban areas. Moreover, in suburban areas, even with high intensities the rain reduces the coverage probability slightly.[9]
- As opposed to the rain and the blockage, depending on the network density, in the cases with low/moderate IABs' densities the coverage probability may be considerably affected by the tree foliage. For instance, consider the parameter settings of Fig. 9, in suburban area, with 1 MBS, $\lambda_U = 50$ km^{-2} and an average hop distance of $l_{hop} = 900$ m, corresponding to $\lambda_S = 3$ km^{-2}. Then, the presence of trees with line length $l_T = 15$ m and density $\lambda_T = 250$ km^{-2} reduces the coverage probability from 70% for the cases with no trees to 60%, i.e., for 10% more of the UEs the rate requirement 50 Mbps can not be provided. Thus, in the presence of tree foliage, more IAB nodes are required to satisfy the same QoS requirement. On the other hand, with high network density, the coverage probability is not affected by the tree foliage (Fig. 9). In general, predicting the link performance for IAB is difficult when accepting foliage. This is because, for instance, the backhaul link quality may change due to wet trees, snow on the trees, wind and varying percentage of leaves in different seasons. However, based on the presented results, we believe that, with appropriate nodes heights, mmWave IAB will work well for areas with low/moderate foliage level.

Finally, it should be mentioned that in Figs. 8-9 we considered the same parameter settings for the IAB nodes, independently of their area of implementation. However, in practice, different types of short-range and wide-area IAB nodes, with considerably higher capabilities for the wide-area IAB nodes, may be developed and used in urban and suburban areas, respectively [63]. This will help to reduce the effect of rain/foliage in suburban areas even more.

4) PERFORMANCE EVALUATION IN AN EXAMPLE 3D USE-CASE

In Figs. 5-9, we investigate the system performance in the 2D FHPPP-based model. To evaluate the effect of the nodes and blockages heights, in this subsection we study the coverage probability in an example 3D setup. Particularly, as shown in Fig. 10, the UEs and the IAB nodes (both MBSs and SBSs) are still randomly distributed based on their corresponding FHPPPs, while they are positioned at different heights. Moreover, the blockages (as well as the distance between the nodes) are determined based on the

9. It should be noted that, while Fig. 8 presents the results for 28 GHz which is the frequency of interest for IAB, the effect of the rain will be more visible at higher carrier frequencies.
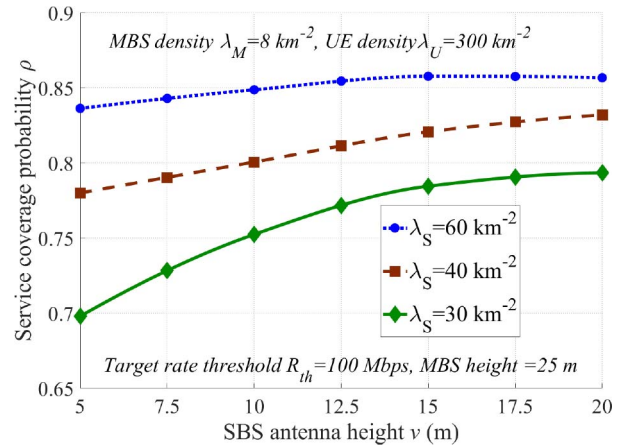
FIGURE 11. Service coverage probability as a function of the SBSs antenna height *v* for the cases with no rain and P_{MBS}, P_{SBS}, P_{UE} = (40, 24, 0) dBm.
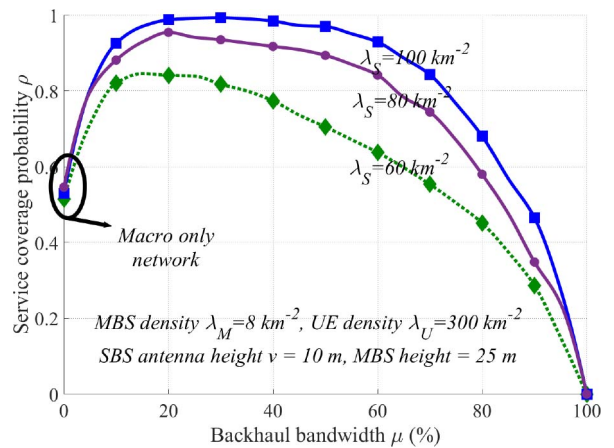
FIGURE 12. Service coverage probability as a function of the backhaul bandwidth allocation percentage μ in (11) for a dense network, no rain, R_{th} = 100 Mbps, and P_{MBS}, P_{SBS}, P_{UE} = (40, 24, 0) dBm.

map information, i.e., the real world blocking terrain is considered using OpenStreetMap 3D environment. The results have been tested on a disk of radius $D = 0.5$ km over the Chalmers University of Technology, Gothenburg, Sweden. Particularly, considering the MBSs and the UEs heights to be 25 and 1 m, respectively, Figs. 11 and 12 show the coverage probability as a function of the SBSs' heights and the backhaul bandwidth allocation percentage, μ in (11), respectively.

As demonstrated in Fig. 11, with a low SBS density, increasing the height of the SBSs helps to reduce the required number of IAB nodes considerably. For instance, with the parameter settings of Fig. 11, the same coverage probability as in the cases with density $\lambda_S = 40$ km^{-2} and height $v = 5$ m is achieved by a setup having $\lambda_S = 30$ km^{-2} and $v = 15$ m. However, as the network density increases, the effect of the SBSs height becomes negligible. This is intuitively because, with moderate/high densities, with high probability one can always find IAB donor-IAB, IAB-UE,

and IAB donor-UE links with strong LOS signal components, even if the IAB nodes are located on the street level.

Finally, as shown in Fig. 12, with an optimal bandwidth allocation between the access and backhaul, IAB network increases the coverage probability, compared to the cases with only MBSs, significantly (Also, see Fig. 6). With $\mu = 0$, the system performance decreases to those achieved by only MBSs, as no bandwidth is allocated for backhauling. With $\mu = 100\%$, on the other hand, no resources are considered for access, and the coverage probability tends to zero. Thus, for different parameter settings, there is an optimal value for the portion of backhaul/access bandwidth allocation maximizing the coverage probability (Fig. 12). Deriving this optimal value, which increases with the SBSs' density and decreases with the UEs' density, is an open research topic for which the results of [27] is supportive.

IV. CONCLUSION

We studied IAB networks from both standardization and performance points of view. As we showed, depending on the QoS requirements, IAB can be considered as a cost-effective alternative to optical fiber that complements conventional microwave backhaul, in different use-cases and areas. Particularly, the same coverage probability as in fiber-connected networks is achieved by relatively small increment in the number of IAB nodes, leading to considerable network cost reduction/flexibility increment. Moreover, unless for the cases with moderate/high tree foliage in suburban areas, the system performance is not much affected by, e.g., the blockage, the rain, and the tree foliage, which introduces the IAB as a robust setup for dense networks.

While the industry has well proceeded in standardization of different aspects of the network, there are still many open research problems to be addressed by the academia. Among such research topics are topology optimization using, e.g., machine learning, studying the effect of hardware impairments on the system performance, developing efficient methods for simultaneous transmission/reception, improving the system performance using network coding, designing efficient (hybrid) beamforming methods for IAB networks, combination of IAB nodes and repeaters/intelligent surfaces, as well as mobile IAB. Also, load balancing and adaptive routing in a mesh-based network are interesting research topics for which the fundamental results of relay networks, e.g., [64]–[66], will be supportive. Although some of these topics are not supported in Rel-16 and 17, a deep analysis of such problems may pave the way for further enhancements of IAB in industry.

REFERENCES

[1] Ericsson. *Mobile Data Traffic Growth Outlook*. Accessed: Mar. 24, 2020. [Online]. Available: https://www.ericsson.com/en/mobility-report/reports/november-2018/mobile-data-traffic-growth-outlook

[2] M. Agiwal, A. Roy, and N. Saxena, "Next generation 5G wireless networks: A comprehensive survey," *IEEE Commun. Surveys Tuts.*, vol. 18, no. 3, pp. 1617–1655, 3rd Quart., 2016.

[3] S. Dang, O. Amin, B. Shihada, and M.-S. Alouini, "What should 6G be?" *Nat. Electron.*, vol. 3, no. 1, pp. 20–29, Jan. 2020.

[4] Ericsson. *Mobile Data Traffic Growth Outlook*. Accessed: Jun. 7, 2020. [Online]. Available: https://www.ericsson.com/en/mobility-report/reports/november-2018/mobile-data-traffic-growth-outlook

[5] C. Czegledi *et al.*, "Demonstrating 139 Gbps and 55.6 bps/Hz spectrum efficiency using 8x8 MIMO over a 1.5 km link at 73.5 GHz," presented at the IMS2020, Aug. 2020.

[6] H. Dahrouj, A. Douik, F. Rayal, T. Y. Al-Naffouri, and M. Alouini, "Cost-effective hybrid RF/FSO backhaul solution for next generation wireless systems," *IEEE Wireless Commun. Mag.*, vol. 22, no. 5, pp. 98–104, Oct. 2015.

[7] C. Dehos, J. L. González, A. D. Domenico, D. Kténas, and L. Dussopt, "Millimeter-wave access and backhauling: The solution to the exponential data traffic increase in 5G mobile communications systems?" *IEEE Commun. Mag.*, vol. 52, no. 9, pp. 88–95, Sep. 2014.

[8] Y. Li, E. Pateromichelakis, N. Vucic, J. Luo, W. Xu, and G. Caire, "Radio resource management considerations for 5G millimeter wave backhaul and access networks," *IEEE Commun. Mag.*, vol. 55, no. 6, pp. 86–92, Jun. 2017.

[9] "Overview of 3GPP release 10, v0.2.1," 3GPP, Sophia Antipolis, France, Rep., Jun. 2016.

[10] O. Teyeb, A. Muhammad, G. Mildh, E. Dahlman, F. Barac, and B. Makki, "Integrated access backhauled networks," in *Proc. IEEE 90th Veh. Technol. Conf. (VTC-Fall)*, Honolulu, HI, USA, Sep. 2019, pp. 1–5.

[11] M. N. Islam, S. Subramanian, and A. Sampath, "Integrated access backhaul in millimeter wave networks," in *Proc. IEEE Wireless Commun. Netw. Conf. (WCNC)*, Mar. 2017, pp. 1–6.

[12] M. N. Islam, N. Abedini, G. Hampel, S. Subramanian, and J. Li, "Investigation of performance in integrated access and backhaul networks," in *Proc. IEEE Conf. Comput. Commun. Workshops (INFOCOM WKSHPS)*, Apr. 2018, pp. 597–602.

[13] Y. Li, J. Luo, R. A. Stirling-Gallacher, and G. Caire. (2019). *Integrated Access and Backhaul Optimization for Millimeter Wave Heterogeneous Networks*. [Online]. Available: https://arxiv.org/abs/1901.04959

[14] Y. Liu, A. Tang, and X. Wang, "Joint incentive and resource allocation design for user provided network under 5G integrated access and backhaul networks," *IEEE Trans. Netw. Sci. Eng.*, vol. 7, no. 2, pp. 673–685, Apr./Jun. 2020.

[15] A. Hasanzade-Zonuzy, I. Hou, and S. Shakkottai, "Broadcasting real-time flows in integrated backhaul and access 5G networks," in *Proc. Int. Symp. Model. Optim. Mobile Ad Hoc Wireless Netw. (WiOPT)*, 2019, pp. 1–8.

[16] M. Polese, M. Giordani, A. Roy, D. Castor, and M. Zorzi, "Distributed path selection strategies for integrated access and backhaul at mmWaves," in *Proc. IEEE Global Commun. Conf. (GLOBECOM)*, Dec. 2018, pp. 1–7.

[17] B. Zhai, M. Yu, A. Tang, and X. Wang, "Mesh architecture for efficient integrated access and backhaul networking," in *Proc. IEEE Wireless Commun. Netw. Conf. (WCNC)*, 2020, pp. 1–6.

[18] J. Y. Lai, W. Wu, and Y. T. Su, "Resource allocation and node placement in multi-hop heterogeneous integrated-access-and-backhaul networks," *IEEE Access*, vol. 8, pp. 122937–122958, 2020.

[19] F. Gómez-Cuba and M. Zorzi, "Twice simulated annealing resource allocation for mmwave multi-hop networks with interference," in *Proc. IEEE Int. Conf. Commun. (ICC)*, 2020, pp. 1–7.

[20] M. N. Kulkarni, A. Ghosh, and J. G. Andrews. (2018). *Max–Min Rates in Self-Backhauled Millimeter Wave Cellular Networks*. [Online]. Available: https://arxiv.org/abs/1805.01040

[21] M. Polese, M. Giordani, A. Roy, S. Goyal, D. Castor, and M. Zorzi, "End-to-end simulation of integrated access and backhaul at mmWaves," in *Proc. IEEE 23rd Int. Workshop Comput.-Aided Model. Design Commun. Links Netw. (CAMAD)*, Barcelona, Spain, Sep. 2018, pp. 1–7.

[22] M. Polese *et al.*, "Integrated access and backhaul in 5G mmWave networks: Potential and challenges," *IEEE Commun. Mag.*, vol. 58, no. 3, pp. 62–68, Mar. 2020.

[23] F. Gomez-Cuba and M. Zorzi, "Optimal link scheduling in millimeter wave multi-hop networks with space division multiple access," in *Proc. IEEE Inf. Theory Appl. Workshop (ITA)*, 2016, pp. 1–9.

[24] M. Hashemi, M. Coldrey, M. Johansson, and S. Petersson, "Integrated access and backhaul in fixed wireless access systems," in *Proc. IEEE 86th Veh. Technol. Conf. (VTC-Fall)*, Toronto, ON, Canada, Sep. 2017, pp. 1–5.

[25] M. N. Kulkarni, J. G. Andrews, and A. Ghosh, "Performance of dynamic and static TDD in self-backhauled millimeter wave cellular networks," *IEEE Trans. Wireless Commun.*, vol. 16, no. 10, pp. 6460–6478, Oct. 2017.

[26] B. Makki, M. Hashemi, L. Bao, and M. Coldrey, "On the performance of FDD and TDD systems in different data traffics: Finite block-length analysis," in *Proc. IEEE 88th Veh. Technol. Conf. (VTC-Fall)*, Aug. 2018, pp. 1–5.

[27] C. Saha, M. Afshang, and H. S. Dhillon, "Integrated mmWave access and backhaul in 5G: Bandwidth partitioning and downlink analysis," in *Proc. IEEE Int. Conf. Commun. (ICC)*, May 2018, pp. 1–6.

[28] S. Singh, M. N. Kulkarni, A. Ghosh, and J. G. Andrews, "Tractable model for rate in self-backhauled millimeter wave cellular networks," *IEEE J. Sel. Areas Commun.*, vol. 33, no. 10, pp. 2196–2211, Oct. 2015.

[29] C. Saha and H. S. Dhillon. (2019). *Millimeter Wave Integrated Access and Backhaul in 5G: Performance Analysis and Design Insights*. [Online]. Available: https://arxiv.org/pdf/1902.06300.pdf

[30] A. Fouda, A. S. Ibrahim, I. Guvenc, and M. Ghosh, "UAV-based in-band integrated access and backhaul for 5G communications," in *Proc. IEEE 88th Veh. Technol. Conf. (VTC-Fall)*, Aug. 2018, pp. 1–5.

[31] N. Tafintsev *et al.*, "Aerial access and backhaul in mmWave B5G systems: Performance dynamics and optimization," *IEEE Commun. Mag.*, vol. 58, no. 2, pp. 93–99, Feb. 2020.

[32] N. Tafintsev *et al.*, "Reinforcement learning for improved UAV-based integrated access and backhaul operation," in *Proc. IEEE Int. Conf. Commun. Workshops (ICC Workshops)*, 2020, pp. 1–7.

[33] S. M. Azimi-Abarghouyi, B. Makki, M. Haenggi, M. Nasiri-Kenari, and T. Svensson, "Coverage analysis of finite cellular networks: A stochastic geometry approach," in *Proc. Iran Workshop Commun. Inf. Theory (IWCIT)*, Tehran, Iran, Apr. 2018, pp. 1–5.

[34] Ericsson. *Long Haul*. Accessed: Jun. 7, 2020. [Online]. Available: https://www.ericsson.com/en/portfolio/networks/ericsson-radio-system/mobile-transport/microwave/long-haul

[35] "NR; Study on integrated access and backhaul," 3GPP, Sophia Antipolis, France, Rep. TR 38.874, Dec. 2018.

[36] *NG-RAN; Architecture Description*, 3GPP Standard TS 38.401, Mar. 2020.

[37] *NR; Backhaul Adaptation Protocol (BAP) Specification*, 3GPP Standard TS 38.340, Apr. 2020.

[38] "CR to 38.401 support for IAB," 3GPP, Sophia Antipolis, France, Mar. 2020.

[39] *RAN1 Agreements for Rel-16 IAB*, document R1-1913600 Meeting #99, 3GPP, Sophia Antipolis, France, Nov. 2019.

[40] *Technical Specification Group Radio Access Network; NG-RAN; F1 Application Protocol (F1AP)*, 3GPP Standard TS 38.473, Mar. 2020.

[41] *Technical Specification Group Radio Access Network; NG-RAN; Architecture Description*, 3GPP Standard TS 38.401, Mar. 2020.

[42] *Draft Meeting Report*, 3GPP, Sophia Antipolis, France, Mar. 2020. [Online]. Available: https://www.3gpp.org/ftp/TSG_RAN/TSG_RAN/TSGR_87e/Report/

[43] *New WID on Enhancements to Integrated Access and Backhaul*, document RP-193251 Meeting #86, 3GPP, Sophia Antipolis, France, Dec. 2019.

[44] *WF on Simulation Assumptions for IAB Co-Existence Study*, document R4-1907825 Meeting RAN4 #91, 3GPP, Sophia Antipolis, France, May 2019.

[45] S. M. Azimi-Abarghouyi, B. Makki, M. Nasiri-Kenari, and T. Svensson, "Stochastic geometry modeling and analysis of finite millimeter wave wireless networks," *IEEE Trans. Veh. Technol.*, vol. 68, no. 2, pp. 1378–1393, Feb. 2019.

[46] B. Błaszczyszyn. (2017). *Lecture Notes on Random Geometric Models—Random Graphs, Point Processes and Stochastic Geometry*. [Online]. Available: https://hal.inria.fr/cel-01654766/document

[47] T. S. Rappaport *et al.*, "Overview of millimeter wave communications for fifth-generation (5G) wireless networks—With a focus on propagation models," *IEEE Trans. Antennas Propag.*, vol. 65, no. 12, pp. 6213–6230, Dec. 2017.

[48] "Physical layer aspects for evolved UTRA," 3GPP, Sophia Antipolis, France, Rep. TR 25.814, Apr. 2020.

[49] "Specific attenuation model for rain for use in prediction methods," Int. Telecommun. Union, Geneva, Switzerland, ITU Recommendation P. 838-3, 2006.

[50] P. J. Diggle, *Some Statistical Aspects of Spatial Distribution Models for Plants and Trees*. Uppsala, Sweden: Swedish Univ. Agricult. Sci., 1982.

[51] M. A. Abu-Rgheff, *5G Physical Layer Technologies*. Hoboken, NJ, USA: Wiley, Nov. 2019, pp. 303–313.

[52] A. Thornburg, T. Bai, and R. W. Heath, "Interference statistics in a random mmwave ad hoc network," in *Proc. IEEE Int. Conf. Acoust. Speech Signal Process. (ICASSP)*, 2015, pp. 2904–2908.

[53] M. Rebato, M. Mezzavilla, S. Rangan, F. Boccardi, and M. Zorzi, "Understanding noise and interference regimes in 5G millimeter-wave cellular networks," in *Proc. 22nd Eur. Wireless Conf.*, 2016, pp. 1–5.

[54] T. A. Khan, A. Alkhateeb, and R. W. Heath, "Millimeter wave energy harvesting," *IEEE Trans. Wireless Commun.*, vol. 15, no. 9, pp. 6048–6062, Sep. 2016.

[55] T. K. Vu, M. Bennis, S. Samarakoon, M. Debbah, and M. Latva-Aho, "Joint load balancing and interference mitigation in 5G heterogeneous networks," *IEEE Trans. Wireless Commun.*, vol. 16, no. 9, pp. 6032–6046, Jun. 2017.

[56] T. M. Shami, D. Grace, A. Burr, and J. S. Vardakas, "Load balancing and control with interference mitigation in 5G heterogeneous networks," *EURASIP J. Wireless Commun. Netw.*, vol. 2019, no. 1, p. 177, 2019.

[57] E. J. Oughton and Z. Frias, *Exploring the Cost, Coverage and Rollout Implications of 5G in Britain*. Cambridge, U.K.: Centre Risk Stud., 2016.

[58] "Deliverable D2.1: Use Cases, Scenarios and Requirements," 5G NORMA, New York, NY, USA, Rep., 2015.

[59] H. A. Willebrand and B. S. Ghuman, "Fiber optics without fiber," *IEEE Spectr.*, vol. 38, no. 8, pp. 40–45, Aug. 2001.

[60] GSMA. *Mobile Backhaul: An Overview*. Accessed: May 1, 2020. [Online]. Available: https://www.gsma.com/futurenetworks/wiki/mobile-backhaul-an-overview/

[61] (Dec. 2019). *AT&T and Verizon to Use Integrated Access and Backhaul for 2021 5G Networks*. [Online]. Available: https://techblog.comsoc.org/2019/12/16/att-and-verizon-to-use-integrated-access-and-backhaul-for-2021-5g-networks

[62] (Oct. 2019). *Verizon to Use 'Integrated Access Backhaul' for Fiber-Less 5G*. [Online]. Available: https://www.lightreading.com/mobile/5g/verizon-to-use-integrated-access-backhaul-for-fiber-less-5g/d/d-id/754752

[63] *WF on IAB-MT class descriptions*, document R4-2008767 Meeting #95-e, 3GPP, Sophia Antipolis, France, May/Jun. 2015.

[64] X. Lin and J. G. Andrews, "Connectivity of millimeter wave networks with multi-hop relaying," *IEEE Wireless Commun. Lett.*, vol. 4, no. 2, pp. 209–212, Feb. 2015.

[65] S. Sharma, Y. Shi, Y. T. Hou, H. D. Sherali, S. Kompella, and S. F. Midkiff, "Joint flow routing and relay node assignment in cooperative multi-hop networks," *IEEE J. Sel. Areas Commun.*, vol. 30, no. 2, pp. 254–262, Jan. 2012.

[66] M. Movahednasab, B. Makki, N. Omidvar, M. R. Pakravan, T. Svensson, and M. Zorzi, "An energy-efficient controller for wirelessly-powered communication networks," *IEEE Trans. Commun.*, vol. 68, no. 8, pp. 4986–5002, Jun. 2020.

CHARITHA MADAPATHA received the B.Sc. degree in telecommunications engineering from the Asian Institute of Technology, Pathumthani, Thailand, in 2016, and the M.Sc. degree in communication engineering from the Chalmers University of Technology, Gothenburg, Sweden, in 2020, where he is currently pursuing the Ph.D. degree in communication systems and information theory.

He has coauthored several international scientific publications in the field of wireless networks. His current research interests include integrated access and backhaul, multiantenna systems, mmWave communication, analysis of physical layer algorithms, and resource allocation. He is a recipient of the Swedish Institute Scholarship for Global Professionals, Sweden, in 2018 and the AIT Fellowship Grant, Thailand, in 2014–2016. He was also involved in LTE network planning and optimization in Thailand and Cambodia.

BEHROOZ MAKKI (Senior Member, IEEE) received the Ph.D. degree in communication engineering from the Chalmers University of Technology, Gothenburg, Sweden.

From 2013 to 2017, he was a Postdoctoral Researcher with the Chalmers University of Technology. He currently works as a Senior Researcher with Ericsson Research, Gothenburg. He has coauthored 57 journal papers, 45 conference papers, and 50 patent applications. His current research interests include integrated access and backhaul, hybrid automatic repeat request, green communications, millimeter-wave communications, free-space optical communication, NOMA, and finite-blocklength analysis and backhauling. He is the recipient of the VR Research Link Grant, Sweden, in 2014, the Ericsson's Research Grant, Sweden, in 2013–2015, the ICT SEED Grant, Sweden, in 2017, as well as the Wallenbergs Research Grant, Sweden, in 2018. He is also a recipient of the IEEE Best Reviewer Award of IEEE TRANSACTIONS ON WIRELESS COMMUNICATIONS in 2018. He currently works as an Editor of IEEE WIRELESS COMMUNICATIONS LETTERS, IEEE COMMUNICATIONS LETTERS, and the *Journal of Communications and Information Networks* as well as an Associate Editor of *Frontiers in Communications and Networks*. He was a member of European Commission Projects "mm-Wave Based Mobile Radio Access Network for 5G Integrated Communications" and "ARTIST4G" as well as various national and international research collaborations.

CHAO FANG received the B.E. degree in communication engineering from Hubei University, Wuhan, China, in 2013, and the M.S. degree in electrical engineering from the Chalmers University of Technology, Gothenburg, Sweden, in 2015, where he is currently pursuing the Ph.D. degree with the Communication Systems Group, Department of Electrical Engineering. His research interests include beamforming, millimeter-wave communication, integrated access backhauled networks, heterogeneous cellular networks, and stochastic geometry.

OUMER TEYEB (Member, IEEE) received the Ph.D. degree in mobile communications from Aalborg University, Denmark, in 2007. Since 2011, he has been working with Ericsson Research, Stockholm, Sweden, where he is currently a Master Researcher. Since 2017, he has been part of the Ericsson 3GPP standardization delegation in the RAN2 WG. He is the inventor/co-inventor of more than 250 patent families, as well as the author/coauthor of several international scientific publications and standardization contributions in the field of wireless networks. His main areas of research are protocol and the architectural aspects of cellular networks, and the interworking of cellular networks with local area wireless networks such as WLAN.

ERIK DAHLMAN is currently a Senior Expert of radio access technologies with Ericsson Research. He has been deeply involved in the development of all 3GPP wireless access technologies, from the early 3G technologies (WCDMA and HSPA), via 4G LTE, and, most recently, the 5G NR technology. His current work is primarily focusing on the evolution of 5G as well as technologies applicable to future beyond 5G wireless access. He has coauthored the books *3G Evolution—HSPA and LTE for Mobile Broadband*, *4G—LTE and LTE-Advanced for Mobile Broadband*, *4G—LTE-Advanced Pro and The Road to 5G*, and, most recently, *5G NR—The Next Generation Wireless Access Technology*.

Dr. Dahlman received the Major Technical Award, an award handed out by the Swedish Government, for his contributions to the technical and commercial success of the 3G HSPA radio-access technology in 2009. In 2010, he was part of the Ericsson team receiving the LTE Award for "Best Contribution to LTE Standards," handed out at the LTE World Summit. In 2014, he was nominated for the European Inventor Award, the most prestigious inventor award in Europe, for contributions to the development of 4G LTE.

MOHAMED-SLIM ALOUINI (Fellow, IEEE) was born in Tunis, Tunisia. He received the Ph.D. degree in electrical engineering from the California Institute of Technology, Pasadena, CA, USA, in 1998. He served as a Faculty Member with the University of Minnesota, Minneapolis, MN, USA, and then with Texas A&M University at Qatar, Doha, Qatar. In 2009, he joined the King Abdullah University of Science and Technology, Thuwal, Saudi Arabia, as a Professor of electrical engineering. His current research interests include modeling, design, and performance analysis of wireless communication systems.

TOMMY SVENSSON (Senior Member, IEEE) received the Ph.D. degree in information theory from the Chalmers University of Technology, Gothenburg, Sweden, in 2003. He has worked at Ericsson AB with core networks, radio access networks, and microwave transmission products. He is a Full Professor of communication systems with the Chalmers University of Technology, where he is leading the wireless systems research on air interface and wireless backhaul networking technologies for future wireless systems. He was involved in the European WINNER and ARTIST4G projects that made important contributions to the 3GPP LTE standards, the EU FP7 METIS and the EU H2020 5GPPP mmMAGIC and 5GCar projects toward 5G and beyond, as well as in the ChaseOn Antenna Systems Excellence Center, Chalmers University of Technology, targeting mm-Wave solutions for 5G access, backhaul/fronthaul, and V2X scenarios. He has coauthored four books, 89 journal papers, 127 conference papers, and 53 public EU projects deliverables. His research interests include design and analysis of physical layer algorithms, multiple access, resource allocation, cooperative systems, moving networks, and satellite networks. He is the Chairman of the IEEE Sweden joint Vehicular Technology/Communications/Information Theory Societies Chapter, and a Founding Editorial Board Member and an Editor of the IEEE JSAC Series on Machine Learning in Communications and Networks. He has been an Editor of IEEE TRANSACTIONS ON WIRELESS COMMUNICATIONS and IEEE WIRELESS COMMUNICATIONS LETTERS, guest editor of several top journals, organized several tutorials and workshops at top IEEE conferences, and served as the Coordinator of the Communication Engineering Master's Program at Chalmers University of Technology.